Geosci. Model Dev. Discuss., https://doi.org/10.5194/gmd-2017-289
Manuscript under review for journal Geosci. Model Dev.
Discussion started: 17 January 2018


Geoscientific Model Development Discussions

# A multilayer approach and its application in modeling QGNSea V1.0: a local gravmetric quasi-geoid model over the North Sea

**Yihao Wu** [1, 2], **Zhicai Luo** [1], **Bo Zhong**[3], **Chuang Xu**[1]

[1] MOE Key Laboratory of Fundamental Physical Quantities Measurement, School of Physics, Huazhong University of Science and Technology, Wuhan, China

[2] State Key Laboratory of Geodesy and Earth's Dynamics, Institute of Geodesy and Geophysics, Chinese Academy of Sciences, Wuhan, China

[3]School of Geodesy and Geomatics, Wuhan University, Wuhan, China

*Correspondence to*: Yihao Wu (yihaowu@hust.edu.cn)

**Abstract:** A multilayer approach is set up for local gravity field modeling based on the idea of multi-resolution representation merging heterogeneous gravity data. Different layers of Poisson wavelets' grids are formed to recover the signals at various levels, where the shallow and deep layers mainly capture the short- and long-wavelength signals, respectively. The depths of these layers beneath the topography are linked to the locations that the anomaly sources locate, estimated by the wavelet decomposition and power spectrum analysis. For testing the performance of this approach, a gravimetric quasi-geoid over the North Sea in Europe called QGNSea V1.0 is computed and compared with other existing models. The results show that the multilayer approach outperforms the traditionally used single-layer one in high-frequency bands, and the former fit the gravity data better, especially in regions with a tendency toward topographical variation. The evaluation with GPS/leveling data show the accuracies of QGNSea V1.0 modeled from the multilayer approach are improved by 0.3 cm, 0.6 cm and 0.8 cm in the Netherlands, Belgium and parts of Germany, respectively, compared to the original solution computed from the single-layer approach. Further validation with existing models show QGNSea V1.0 has the best quality, which may be beneficial for studying the ocean circulation between the North Sea and neighbouring waters.

## 1. Introduction

Knowing of earth's gravity field at regional scales is crucial for a variety of applications in geodesy. It not only facilitates the use of Global Satellite Navigation System to determine orthometric/normal heights in geodesy and surveying engineering, but also plays a fundamental role in in oceanography and geophysics.

Geosci. Model Dev. Discuss., https://doi.org/10.5194/gmd-2017-289
Manuscript under review for journal Geosci. Model Dev.
Discussion started: 17 January 2018




Spherical radial basis functions (SRBFs) are of great interest for gravity field modeling at regional scales over years (Eicker et al., 2013; Naeimi et al., 2015). Typically, the widely-used SRBFs method is implemented by the so-called single-layer approach, i.e., the parameterization of gravity field is only based on a single-layer of SRBFs' grid (Wittwer, 2009; Bentel et al., 2013; Wu et al., 2017b). However, one layer of SRBF's parameterization may be only sensitive to parts of signals' spectrum and reduce the quality of the solution.

Contrary to the single-layer approach, SRBFs are also of special interest for multi-resolution representation (MRR) for merging different spectral contents of complementary observations techniques (Freeden et al., 1998; Fengler et al., 2004, 2007). The motivation behind this is the feasibility to compute the signals at different scales independently, and the ability to identify the certain geophysical features at the different spectral bands (Wittwer, 2009). Freeden and Schreiner (2006) proposed a multi-scale approach based on the locally supported wavelets for determining the regional geoid undulations from the deflections of the vertical. Freeden et al. (2009) demonstrated that the multi-scale approach using spherical wavelets provided local fine-structured features such as those caused by plumes, which allowed a scale- and space-dependent characterization of this geophysical phenomenon. Schmidt et al. (2005, 2006, 2007) developed a multi-representation method for static and spatiotemporal gravity field modeling through SRBFs, where the input gravity signals were decomposed into a certain number of frequency-dependent detail signals, and concluded that this approach could improve the spanning fixed time intervals with respect to the usual time-variable gravity fields. Chambodut et al. (2005) set up a multi-scale method for magnetic and gravity field recovery using Poisson wavelets, and created a set of hierarchical meshes associated with the wavelets at different scales, where a level of subdivision corresponded to a given wavelet scale. Panet et al. (2011) extended the approach developed by Chamboudt et al. (2005), and applied a domain decomposition approach to define the hierarchical subdomains of wavelets at different scales, which allowed to split a large problem into smaller ones. These results show the multi-scale approach with SRBFs has a good prospective in gravity field modeling using heterogeneous data. However, differing from these methods mentioned above, we propose a multilayer approach, inspired by the power spectral analysis of local gravity observations, which indicates the gravity signals are the sum of the contributions generated from the anomaly sources that locate at different depths.

The structure of the manuscript is as follows: the heterogeneous data in a study area in Europe are firstly described in Section 2. Then, the multilayer approach is introduced, and the wavelet decomposition and power spectrum analysis

Geosci. Model Dev. Discuss., https://doi.org/10.5194/gmd-2017-289
Manuscript under review for journal Geosci. Model Dev.
Discussion started: 17 January 2018




are applied for estimating the depths of various layers beneath the topography. In addition, we set up the function model based on the multilayer approach and combine the different types of gravity data. We construct the networks of multiply layers in section 3, and compare the performances of different approaches. Finally, the solution called QGNSea V1.0 is modeled by the multilayer approach and compared with other existing models for evaluating the additional values introduced by this approach. We summarize the main summaries and conclusions of this study in section 4.

# 2. Data and method

## 2.1. Study area and data

A local region in Europe is chosen as a case study, which covers an area of 49 ℃N-61 ℃N latitude and -6 ℃E-10 ℃E longitude, including the mainland of the Netherlands, Belgium, and parts of the North Sea, UK, Germany and France. Point-wise terrestrial and shipborne gravity anomalies are incorporated for testing the approach we developed in this study, which were provided by different institutions, see Slobbe et al. (2014). The details for data pre-processing procedures can be found in Wu et al. (2017b), where crossover adjustment and low-pass filter were applied to remove systematic errors and reduce high-frequency noise, respectively, and datum transformations were performed on all the data. Moreover, the satellite-only reference model called GOCO05s with a full degree and order (d/o) of 280 (Mayer-Gürr et al., 2015) and RTM corrections were removed from the original observations to decrease the signal correlation length and smooth the data within the framework of remove-compute-restore (RCR) framework, and the details for the RTM reduction and residual gravity data could be found in Wu et al. (2017b).

## 2.2. Multilayer approach

According to Schmidt et al. (2006, 2007), the multi-resolution representation (MRR) of the Earth's potential $T(\boldsymbol{z})$ on position $\boldsymbol{z}$ is expressed as

$$T(\boldsymbol{z}) = \bar{T}(\boldsymbol{z}) + \sum_{i=1}^{I} t_i(\boldsymbol{z}) + \delta(\boldsymbol{z}) \quad (1)$$

where $T(\boldsymbol{z})$ is the disturbing potential in this study, $\bar{T}(\boldsymbol{z})$ means a reference model, e.g., a global geopotential model (GGM) computed from spherical harmonics; $\delta(\boldsymbol{z})$ represents the unmodeled signals; $I$ is the number of levels (resolutions); $t_i(\boldsymbol{z})$ is the detailed signal of level $i$, and the higher the level value $i$ is, the finer are the structures

Geosci. Model Dev. Discuss., https://doi.org/10.5194/gmd-2017-289
Manuscript under review for journal Geosci. Model Dev.
Discussion started: 17 January 2018




extractable from the input data; $t_i(\boldsymbol{z})$ is computed as the a linear combination of SRBFs (Schmidt et al., 2007)

$$t_i(\boldsymbol{z}) = \sum_{k=1}^{K_i} \beta_{i,k} \Psi_i(\boldsymbol{z}, \boldsymbol{y}_{i,k}) \tag{2}$$

where $\Psi(\boldsymbol{z}, \boldsymbol{y})$ is the SRBF, $K_i$ and $\beta_{i,k}$ are the number and unknown coefficients of SRBFs at level $i$, respectively, and $\boldsymbol{y}_{i,k}$ is the position of SRBF at this level.

We work with the RCR technique, and the reference GGM and RTM corrections are removed from the original data to decrease the signal correlation length and smooth the data (Omang and Forsberg, 2000). Then, only the residual gravity potential $T_{res}(\boldsymbol{z})$ is parameterized by SRBFs using the MRR approach. Neglecting the unmodeled signals, the residual potential is expressed as a series of the detailed signals at different levels when combining Eq.(1) and (2)

$$T_{res}(\boldsymbol{z}) = \sum_{i=1}^{I} \sum_{k=1}^{K_i} \beta_{i,k} \Psi_i(\boldsymbol{z}, \boldsymbol{y}_{i,k}) \tag{3}$$

where $\Psi_i$ is computed as the difference of the spherical scaling functions with low-pass filter characteristics between the consecutive levels $i+1$ and $i$, but also can be expressed as the SRBF has the band-limited properties in the frequency domain (Schmidt et al., 2007). In this study, $\Psi$ is chosen as the Poisson wavelet with band-limited properties in the frequency domain (Chambodut et al., 2005), and its full definition can be found in Holschneider and Iglewska-Nowak (2007).

Poisson wavelets can also be identified as the multipoles inside the Earth, and the scales of Poisson wavelets can be related to their depths, which are the key issues that determine their properties in space and frequency domain (Chambodut et al., 2005). The detailed signal at level $i$ in Eq.(3) can be estimated by a linear combination of Poisson wavelets located at a specific depth. Poisson wavelets at depths demonstrate different properties in the frequency domain, as the depths going shallower, the scales decrease, and their spectrums shift towards the high degrees of the spherical harmonics (SH) and become more sensitive to the local features of signals with high-frequency properties, and vice versa (Chambodut et al., 2005). These properties are crucial for local gravity field modeling. First, the

Geosci. Model Dev. Discuss., https://doi.org/10.5194/gmd-2017-289
Manuscript under review for journal Geosci. Model Dev.
Discussion started: 17 January 2018




residual disturbing potential is typically the band-limited signal under the RCR framework, and Poisson wavelets with band-pass filter characteristics are preferable for band-limited signal recovery (Bentel et al., 2013). Moreover, Poisson wavelets at different depths can be linked to the detailed signals at various levels, which are sensitive to different spectral contents of input signals, and could be used for multi-resolution representation.

Rather than using the name of MRR, we interpret Eq.(3) as the multilayer approach considering Poisson wavelets at different depths have various characteristics, and the different layers are corresponding to the Poisson wavelets' grids at various depths. Poisson wavelets are placed on the Fibonacci grids under the topography, and these grids are also kept parallel with the topography (Tenzer et al., 2012). Instead of associating the Poisson wavelets at different depths to the hierarchical meshes with various levels (Chambodut et al., 2005), we apply a wavelet analysis approach to estimate the depths of multiply layers, inspired by the power spectrum analysis of the residual gravity field. The green curve in Figure 1 shows the radially averaged power spectrum of the local gravity field using the data mentioned in sect. 2.1, the slopes of which change in different frequency bands (see the red straight lines), indicating the gravity signals are the superstition of the contributions generated from the anomaly sources at different depths; and the signals originated from different anomaly sources have heterogeneous spectral contents (Spector and Grant, 1970; Syberg, 1972). Since Poisson wavelets at different depths are sensitive to signals with heterogeneous frequency characteristics, and we put Poisson wavelets' grids at the locations where the anomaly sources situate. In this manner, the contributions from the anomaly sources at various depths can be estimated by different layers.

Geosci. Model Dev. Discuss., https://doi.org/10.5194/gmd-2017-289
Manuscript under review for journal Geosci. Model Dev.
Discussion started: 17 January 2018


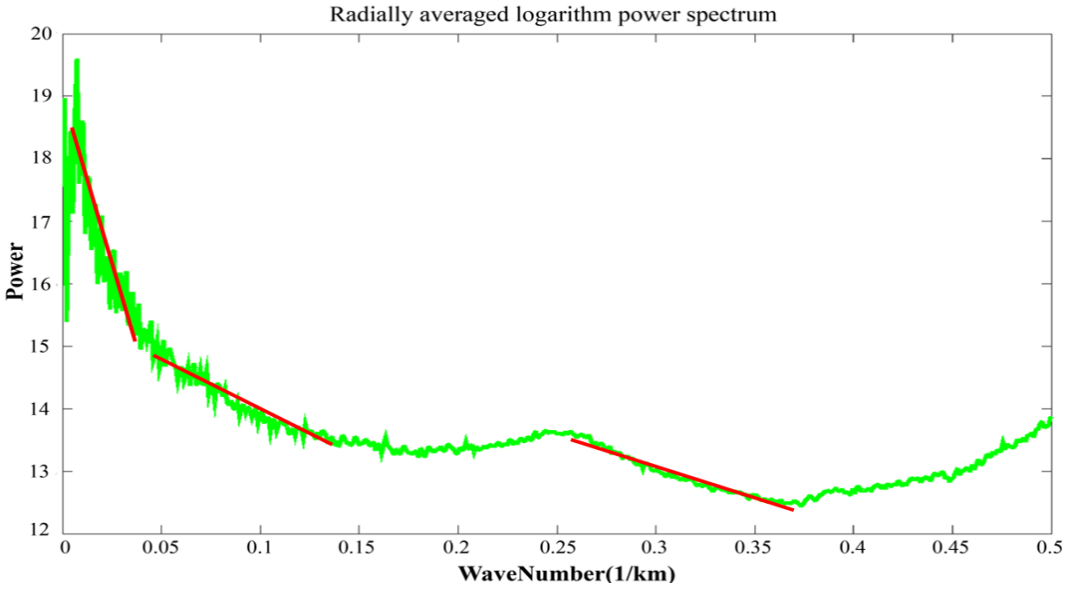


Figure 1. Power spectrum analysis of local gravity field. The green curve is the radially averaged power spectrum, and the red straight lines represent the slopes of the spectrum in different frequency bands

In order to separate the contributions stemmed from different anomaly sources, the wavelet multi-scale analysis, which is an excellent approach to extract the signals at different scales, is applied to decompose the gravity data $\Delta g$ into wavelet approximation $A_W$ and wavelet details $D_w$ $(w = 1, 2, 3, \cdots W)$ at different scales (Jiang et al., 2012; Audet, 2013; Xu et al., 2017)

$$\Delta g = A_W + \sum_{w=1}^{W} D_w \tag{4}$$

where $W$ is the maximum order for decomposition; $A_W$ is the regional anomaly caused by deep and large-scale geological bodies, $D_w$ is the local anomaly originated from shallow and small-scale heterogeneous substances. Wavelets analysis generates low-order wavelet details that are invariant with the decomposition order, and only the high-order wavelet details and corresponding wavelet approximation change with the decomposition order. Based on this property, we can choose the proper decomposition order to derive the desirable solutions.

Geosci. Model Dev. Discuss., https://doi.org/10.5194/gmd-2017-289
Manuscript under review for journal Geosci. Model Dev.
Discussion started: 17 January 2018


Geoscientific Model Development Discussions

The decomposed signals reveal the features of geological bodies, the average depths of which can be estimated from the power spectral analysis (Spector and Grant, 1970; Syberg, 1972; Cianciara and Marcak, 1976)

$$h_w = \frac{1}{4\pi}\frac{\Delta \ln P_k^w}{\Delta k_w} \quad w = 1,2,...,W \tag{5}$$

where $h_w$ is the average depth of anomaly source corresponding to wavelet detail $D_w$; $\ln P_k^w$ is the logarithmic power spectrum of $D_w$; $\Delta \ln P_k^w$ and $\Delta k_w$ are the change rates for $\ln P_k^w$ and radial wave number $k_w$, respectively.

Terrestrial and shipborne gravity anomalies are merged for modeling. Gravity anomalies $\Delta g$ and quasi-geoid height $\zeta$ are related to the disturbing potential based on the multilayer approach as follows:

$$\begin{aligned}\Delta g(\boldsymbol{z}) &\approx -\frac{2}{|\boldsymbol{z}|}T_{res}(\boldsymbol{z}) - \frac{\partial T_{res}(\boldsymbol{z})}{\partial |\boldsymbol{z}|} \\ &= \sum_{i=1}^{I}\sum_{k=1}^{K_i}\beta_{i,k}\left(-\frac{\partial}{\partial |\boldsymbol{z}|}\Psi_i(\boldsymbol{z},\boldsymbol{y}_{i,k}) - \frac{2}{|\boldsymbol{z}|}\Psi_i(\boldsymbol{z},\boldsymbol{y}_{i,k})\right) \\ \zeta(\boldsymbol{z}) &= \frac{T_{res}(\boldsymbol{z})}{\gamma(\boldsymbol{z})} = \sum_{i=1}^{I}\sum_{k=1}^{K_i}\beta_{i,k}\frac{\Psi_i(\boldsymbol{z},\boldsymbol{y}_{i,k})}{\gamma(\boldsymbol{z})}\end{aligned} \tag{6}$$

where $\gamma$ is the normal gravity value.

We suppose the observational errors are white noises with zero mean, and the gravity field model using the multilayer approach is written as the standard Gauss-Markov model

$$\boldsymbol{l}_j - \boldsymbol{e}_j = \boldsymbol{A}_j\boldsymbol{x},\ E\{\boldsymbol{e}_j\} = 0,\ \mathrm{D}\{\boldsymbol{e}_j\} = \boldsymbol{C}_j = \sigma_j^2\boldsymbol{Q}_j = \sigma_j^2\boldsymbol{P}_j^{-1} \tag{7}$$

where $\boldsymbol{x}$ is the $K\times 1$ vector of unknown coefficients, including the unknown parameters of Poisson wavelets from all the layers, i.e., $\boldsymbol{x} = \left[\beta_{1,1},\beta_{1,2},\cdots,\beta_{1,K_1},\beta_{2,1},\beta_{2,2},\cdots,\beta_{2,K_2},\cdots,\beta_{I,1},\beta_{I,2},\beta_{I,K_I}\right]'$, and $K = K_1 + K_2 + \cdots + K_I$; $\boldsymbol{A}_j$ is the $m_j \times K$ design matrix of group $j$, $\boldsymbol{l}_j$ is the $m_j \times 1$ corresponding observation vector, $\boldsymbol{e}_j$ is the $m_j \times 1$ vector of corresponding stochastic errors, and $m_j$ is the number of observations in group $j$. $E\{\cdot\}$ and $D\{\cdot\}$ are

Geosci. Model Dev. Discuss., https://doi.org/10.5194/gmd-2017-289
Manuscript under review for journal Geosci. Model Dev.
Discussion started: 17 January 2018




the expectation and dispersion operators, respectively. $\boldsymbol{C}_j$ is the error variance-covariance matrix of group $j$, and $\sigma_j^2$, $\boldsymbol{Q}_j$ and $\boldsymbol{P}_j$ are the variance factor, cofactor matrix, and weight matrix of group $j$, respectively.

Data in different groups are assumed to be independent, and the weight matrix $\boldsymbol{P}_j$ is supposed to be the scaled diagonal matrix with white noise properties since it is usually difficult to acquire the realistic full error variance-covariance matrix in real-life measurements. Point-wise data can be directly combined for modeling through the functional described above. However, the heterogeneous characteristics for the data, in terms of spatial coverage and noise properties, may result in an ill-conditioned normal matrix (Panet et al., 2011). We apply the first-order Tikhonov regularization for tackling the ill-conditioned problem (Kusche and Klees, 2002; Wu et al., 2017a). For a given $\alpha$ (regularization parameter) and $\kappa$ (regularization matrix), the least-squares solution of Eq.(7) is (Klees et al., 2008):

$$\hat{\boldsymbol{x}} = \left( \sum_{j=1}^{J} \left( \frac{1}{\sigma_j^2} \boldsymbol{A}_j^T \boldsymbol{P}_j \boldsymbol{A}_j \right) + \alpha\kappa \right)^{-1} \left( \sum_{j=1}^{J} \left( \frac{1}{\sigma_j^2} \boldsymbol{A}_j^T \boldsymbol{P}_j \boldsymbol{l}_j \right) \right) \tag{8}$$

Moreover, we use the Monte-Carlo variance component estimation to estimate the appropriate variance factors of various observation groups and the regularization parameter (Koch and Kusche, 2002; Kusche, 2003).

# 3. Numerical results and discussion

## 3.1. Wavelet analysis of local gravity signals

In order to determine the depths of different layers, the residual gravity data are decomposed into the signals at different scales based on wavelets analysis. The spline interpolation is used to compute the gridded data for wavelets decomposition. Coif3 basis functions are chosen for wavelet decomposition (Xu et al., 2017). Figure 2 shows the wavelet details, where the maximum order for decomposition is preliminarily chosen as ten. With the increase of decomposition order, more long-wavelength features show up. More specifically, the low-order details demonstrate the high-frequency signals stemmed from the shallow and small-scale substances. While, the high-order ones with long-wavelength patterns reflect the anomalies caused by deep and large-scale geological bodies. It is noticeable that the 1st- and 2nd-order details ($D_1$ and $D_2$) are seems dominated by the high-frequency signals correlate strongly with

Geosci. Model Dev. Discuss., https://doi.org/10.5194/gmd-2017-289
Manuscript under review for journal Geosci. Model Dev.
Discussion started: 17 January 2018




the local topography (the local digital terrain model (DTM) could be found in Figure 1 in Wu et al., 2017b). We mainly attribute this to the uncorrected signals in RTM corrections, which is due to the inaccuracy of the density parameters in RTM corrections and limitation of DTM both in terms of spatial resolution and precision. As a result, the small-scale signals originated from local topography variation cannot thoroughly recovered from RTM reduction, and the uncorrected signals leak into the 1st- and 2nd-order details. However, these signals are of small magnitude (see Table 1), and we neglect the first two wavelet details for designing the multiply layers' networks to avoid the adverse impacts introduced by these high-frequency noises. Moreover, with the order increasing to nine and larger, we notice $D_9$ and $D_{10}$ obviously reveal the large-scale signals with the wavelengths of hundreds of kilometers. Given that the mean distance between the data is approximately several kilometers and the spatial resolution of the applied GGM is roughly 72 km, the spectral contents of the residual signals is roughly between several kilometers and tens of kilometers within the RCR framework, i.e., approximately between degree 250 to 3000 in terms of spherical harmonics' representation. While, the spectral contents of the 9th- and 10th-order details exceed the frequency bands of the signals need to be recovered, and the maximum order for wavelet decomposition is truncated to eight. In this manner, $D_3$ - $D_8$ and the final wavelet approximation $A_8$ (Figure 3 and Table 2) are applied for constructing multiply layers' networks, which are consist of seven layers at various depths. Different layers are sensitive to signals with heterogeneous frequency characteristics, and shallow and deep layers mainly capture the short- and long-wavelength signals, respectively.

Geosci. Model Dev. Discuss., https://doi.org/10.5194/gmd-2017-289
Manuscript under review for journal Geosci. Model Dev.
Discussion started: 17 January 2018


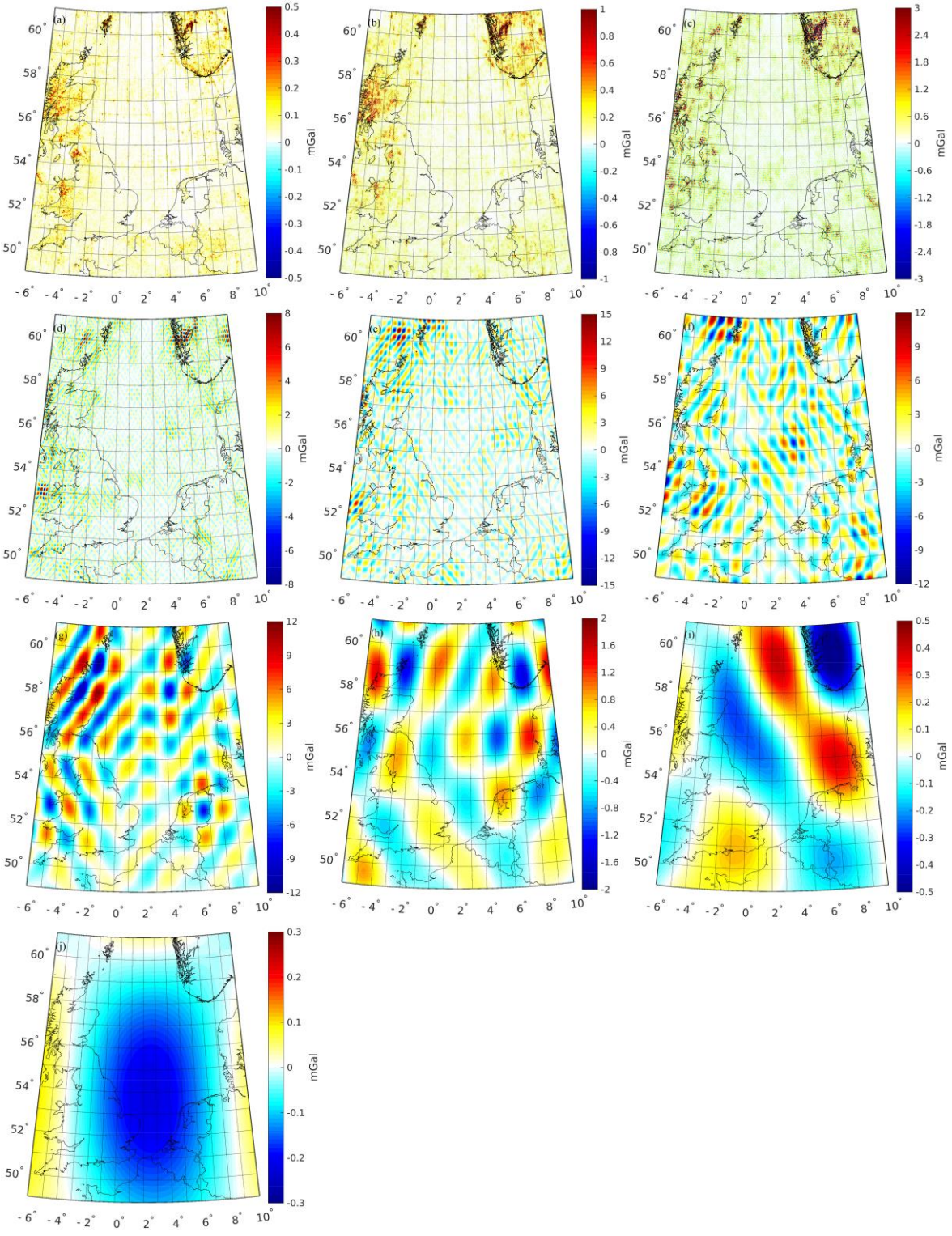

Geosci. Model Dev. Discuss., https://doi.org/10.5194/gmd-2017-289
Manuscript under review for journal Geosci. Model Dev.
Discussion started: 17 January 2018


Geoscientific Model Development Discussions

Figure 2. Wavelet details at various scales. (a) $D_1$, (b) $D_2$, (c) $D_3$, (d) $D_4$, (e) $D_5$, (f) $D_6$, (g) $D_7$, (h) $D_8$, (i) $D_9$ and (j) $D_{10}$

Table 1. Statistics of various wavelet details (units: mGal)

| | max | min | mean | sd |
|---|---|---|---|---|
| $D_1$ | 0.47 | -0.42 | 0.00 | 0.18 |
| $D_2$ | 0.93 | -0.80 | 0.00 | 0.27 |
| $D_3$ | 2.99 | -3.00 | 0.00 | 0.46 |
| $D_4$ | 7.56 | -7.57 | 0.00 | 0.86 |
| $D_5$ | 14.10 | -14.35 | 0.00 | 1.67 |
| $D_6$ | 10.68 | -11.52 | 0.00 | 2.17 |
| $D_7$ | 11.27 | 12.00 | 0.00 | 2.93 |
| $D_8$ | 1.55 | -1.44 | 0.00 | 0.49 |
| $D_9$ | 0.42 | -0.43 | -0.02 | 0.35 |
| $D_{10}$ | 0.29 | -0.24 | -0.13 | 0.15 |

Geosci. Model Dev. Discuss., https://doi.org/10.5194/gmd-2017-289
Manuscript under review for journal Geosci. Model Dev.
Discussion started: 17 January 2018


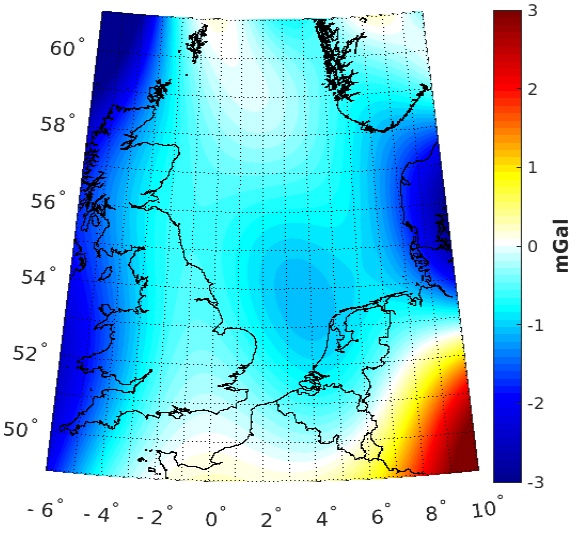


Figure 3. Wavelet approximation $A_8$

Table 2. Statistics of wavelet approximation (units: mGal)

| max | min | mean | sd |
|---|---|---|---|
| 2.23 | -2.40 | -0.43 | 0.53 |

## 3.2. Key parameters of Poisson wavelets

The order of Poisson wavelets is fixed at 3 to achieve a good compromise between the localization in space and frequency domain (Panet et al. 2011). In addition, the depth and number of Poisson wavelets are the crucial points affecting the solution quality (Klees et al. 2008). Poisson wavelets belong to different layers are placed on the Fibonacci grids at various depths beneath the topography, and the power spectrum analysis is applied to estimate the depths. As shown in Figure 4, the green curves show the radially averaged power spectrums for the signals of different scales, and the red straight lines represent the slopes of the spectrums, indicating the depths of corresponding layers. The layers going deeper as the scales increase, and the shallow layers reflect the small-scale signals, while the deep ones recover the long-wavelength information. Table 3 provides the estimated depths for different layers, which are limited between 5 km and 61 km. The shallowest layer locates 5.7 km underneath the topography, while the depth of the deepest one is approximately estimated as 60.2 km. It is noticeable that the thickness of sediments in this target area is approximately 2~4 km, and the thickness of the upper-middle crust is roughly 15~20 km (Artemieva and Thybo 2013). Thus, the first four layers (layer1, layer2, layer3 and layer4) locate between the sediments and upper-middle

Geosci. Model Dev. Discuss., https://doi.org/10.5194/gmd-2017-289
Manuscript under review for journal Geosci. Model Dev.
Discussion started: 17 January 2018




crust, and the corresponding wavelet details ( $D_3$ , $D_4$ , $D_5$ and $D_6$ ) display as the small-scale patterns due to the highly heterogeneous structure of the crust. While, the last three layers (layer5, layer6, and layer7) are supposed to be located between the Moho surface and upper mantle considering the Moho depth in this region is approximately 30 km (Grad and Tiira 2009), and the corresponding details ( $D_7$ , $D_8$ and $A_8$ ) become smoother and more long-wavelength signals show up.

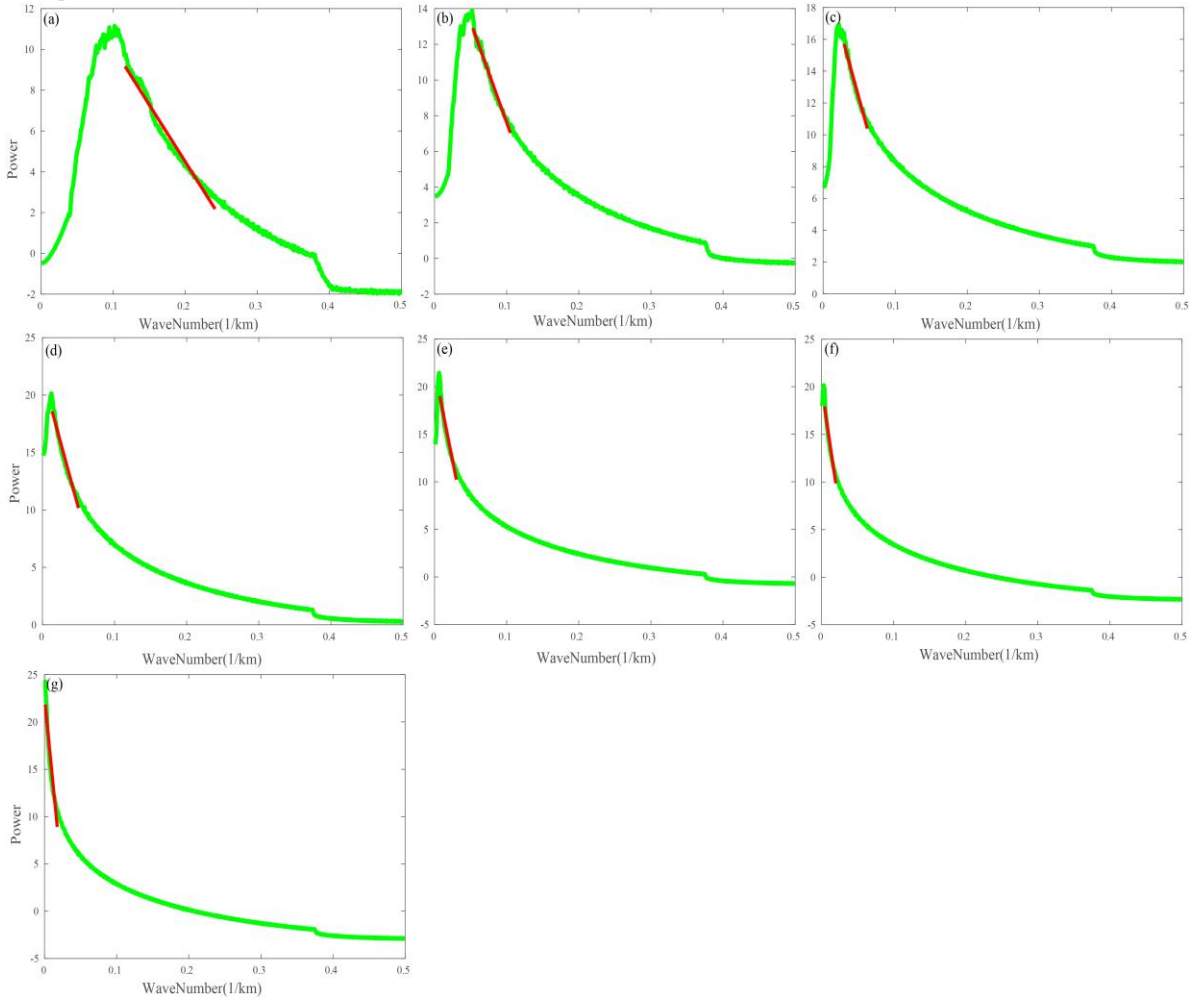


Figure 4. Power spectrum analysis of various wavelet signals. (a) $D_3$ , (b) $D_4$ , (c) $D_5$ , (d) $D_6$ , (e) $D_7$ , (f) $D_8$ , and (g) $A_8$ . The green curves are the radially averaged power spectrums, and the red straight lines represent the slopes of the spectrums.

Geosci. Model Dev. Discuss., https://doi.org/10.5194/gmd-2017-289
Manuscript under review for journal Geosci. Model Dev.
Discussion started: 17 January 2018




Table 3 Depths of multiply layers beneath the topography (Units: km)

| | |
|---|---|
| layer1 | 5.7 |
| layer2 | 10.3 |
| layer3 | 15.1 |
| layer4 | 20.1 |
| layer5 | 32.2 |
| layer6 | 42.7 |
| layer7 | 60.2 |

As mentioned above, different layers are constructed to recover the signals with various spectral contents, and a trial-and-error approach is used to estimate the number of Poisson wavelets for each layer (Wittwer 2009). For a specific layer with the fixed depth, we predefine different number of Poisson wavelets to form a certain number of Fibonacci grids. Then, the signals reconstructed from these grids are compared with the true values, i.e., ones derived from wavelet decomposition, and the parameter that derives the smallest difference between the modeled and true signals is consider as the optimal one. By trail and errors, the spatial resolutions of Fibonacci grids (mean distance between Poisson wavelets) are changed from 20 to 14 km with a step of 1 km. Table 4 shows the accuracies of the solutions derived from different Fibonacci grids for various layers, and we take the situations of the first layer for instance. With more Poisson wavelets, the SD value of the difference between the reconstructed and true signals decreases gradually to 0.10 mGal when the spatial resolution of the grid increase to 16 km. Since then, no significant improvements show up with more Poisson wavelets. Moreover, introducing more Poisson wavelets increases the overlapping between them, which may lead to the highly-conditioned normal matrices, and the associated heavy regularization may decrease the solution quality (Wu et al., 2017a). The optimal mean distance between Poisson wavelets of the first layer is estimated as 14 km. Similarly, the spatial resolutions for the rest layers can be determined in this way, see Table 4.

Geosci. Model Dev. Discuss., https://doi.org/10.5194/gmd-2017-289
Manuscript under review for journal Geosci. Model Dev.
Discussion started: 17 January 2018


Geoscientific Model Development Discussions

Table 4 Accuracies of solutions derived from different Fibonacci grids with various spatial resolutions for different layers (Units: mGal)

| | 20 km | 19 km | 18 km | 17 km | 16 km | 15 km | 14 km |
|---|---|---|---|---|---|---|---|
| layer1 | 0.47 | 0.35 | 0.29 | 0.19 | 0.10 | 0.10 | 0.10 |
| layer2 | 0.32 | 0.30 | 0.28 | 0.26 | 0.23 | 0.15 | 0.15 |
| layer3 | 0.38 | 0.30 | 0.25 | 0.17 | 0.13 | 0.10 | 0.10 |
| layer4 | 0.49 | 0.38 | 0.31 | 0.23 | 0.12 | 0.12 | 0.12 |
| layer5 | 0.28 | 0.20 | 0.15 | 0.13 | 0.12 | 0.10 | 0.10 |
| layer6 | 0.18 | 0.14 | 0.12 | 0.10 | 0.09 | 0.08 | 0.08 |
| layer7 | 0.14 | 0.12 | 0.11 | 0.10 | 0.08 | 0.08 | 0.08 |

### 3.3. Regional solution and its validation

Point-wise terrestrial and shipboard gravity anomalies are merged for modeling. The performance of the traditionally-used single-layer is also investigated for comparison. By trial and errors, the single layer of Poisson wavelets' grid is located 40 km beneath the topography, and the mean distance between Poisson wavelets is defined as 8.7 km (Wu et al., 2016). Figure 5 shows the normalized spectrums for different approaches. Considering the frequency range of the signals to be recovered in the target area is approximately between degree 250 to 3000 in spherical harmonics' representation, we note the single-layer approach is only sensitive to parts of the signals' spectrum, i.e., approximately between degree 300 to 1200 if we suppose half of the maximum value of the normalized spectrum is the criterion for determining whether it is sensitive or not within a specific frequency band. However, for the high-frequency band between degree 1200 to 3000, this approach is less sensitive. On the contrary, the multilayer approach effectively covers the spectrum of the local gravity signals, which is both sensitive to the low- and high-frequency bands. Figure 6 provides the residuals of data after least squares adjustment using different methods, showing the residuals derived from the multilayer approach reduce significantly in the whole region compared with ones obtained from the single-layer approach, especially in western parts of UK, south of Norway, and southwest of Germany, where the high-frequency signals correlated with local topography dominate the features of regional gravity field. We also find the improvements occurring in the ocean parts, especially in waters around the English Channel, Irish Sea, northwest of North Sea, and Atlantic Ocean close to northwest UK. These results demonstrate that the

Geosci. Model Dev. Discuss., https://doi.org/10.5194/gmd-2017-289
Manuscript under review for journal Geosci. Model Dev.
Discussion started: 17 January 2018




multilayer approach can more accurately recovers the local high-frequency signals than the single-layer one. The main reason is that the spectrum of the multilayer method covers the whole spectral contents of the regional gravity signals, which is more sensitive to the high-frequency signals. The statistics in Table 5 displays the SD value for the residuals of terrestrial (shipborne) gravity anomalies decreases by 0.30 mGal (0.34 mGal) when the multilayer approach is used.

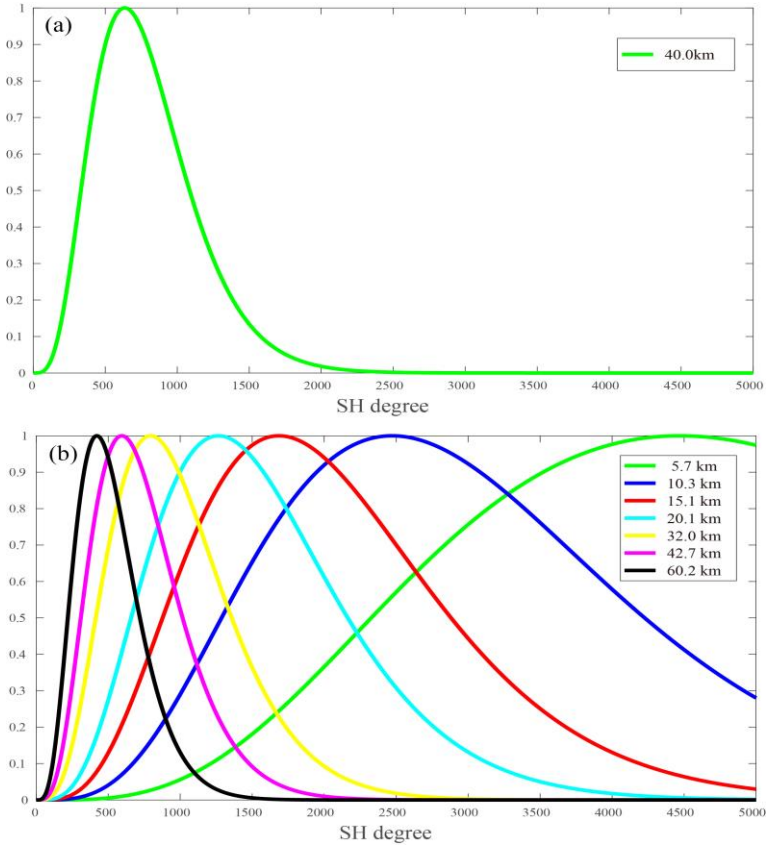


Figure 5. Normalized spectrums for (a) single-layer and (b) multilayer approach

GPS/leveling data in the Netherlands, Belgium, and parts of Germany are used as the validation data, and the results demonstrate the discrepency between the GPS/leveling points and quasi-geoid heights derived from the multilayer approach decrease substantially compared with ones computed from the single-layer approach, see Figure 7. The most prominent improvements occur in the northwest of Belgium, west of Germany, and eastern parts of Netherlands, which are in good agreement with the results for the gravity residuals demonstrated in Figure 6. As shown in Table 6, the accuracies of gravimetric quasi-geoid derived from the multilayer approach are improved by 0.3 cm, 0.6 cm and 0.8

Geosci. Model Dev. Discuss., https://doi.org/10.5194/gmd-2017-289
Manuscript under review for journal Geosci. Model Dev.
Discussion started: 17 January 2018


cm in the Netherlands, Belgium and parts of Germany, respectively. Moreover, the mean values indicate that the solution with the multilayer approach also reduce the biases between gravimetric solution and local GPS/leveling data, with the magnitude of 0.5 cm, 0.7 cm, and 0.7 cm in these three regions, respectively. Based on the evaluation results, we conclude the multilayer approach proposed in this study outperforms the traditionally-used single-layer method, which maybe more preferable in gravity field modeling using heterogeneous data. In following study, we use the model derived from the multilayer approach, which is hereafter denoted as QGNSea V1.0 (quasi-geoid over the North Sea version 1.0).

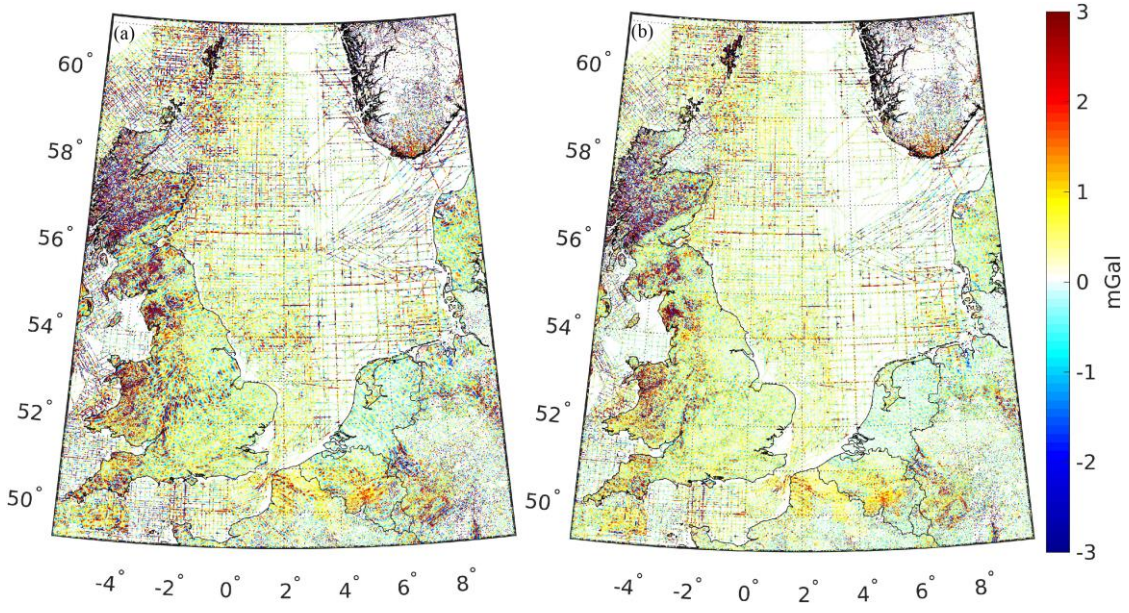


Figure 6. Residuals of gravity data derived from (a) single-layer and (b) multilayer approach

Table 5 Statistics of the residuals of gravity data computed from different approaches (units: mGal)

| | | max | min | mean | sd |
|---|---|---|---|---|---|
| Single-layer approach | Terrestrial | 19.58 | -16.91 | 0.00 | 1.45 |
| | Shipborne | 11.91 | -17.38 | 0.00 | 1.07 |
| Multilayer approach | Terrestrial | 17.41 | -15.83 | 0.00 | 1.15 |
| | Shipborne | 9.50 | -16.75 | 0.00 | 0.73 |

Geosci. Model Dev. Discuss., https://doi.org/10.5194/gmd-2017-289
Manuscript under review for journal Geosci. Model Dev.
Discussion started: 17 January 2018


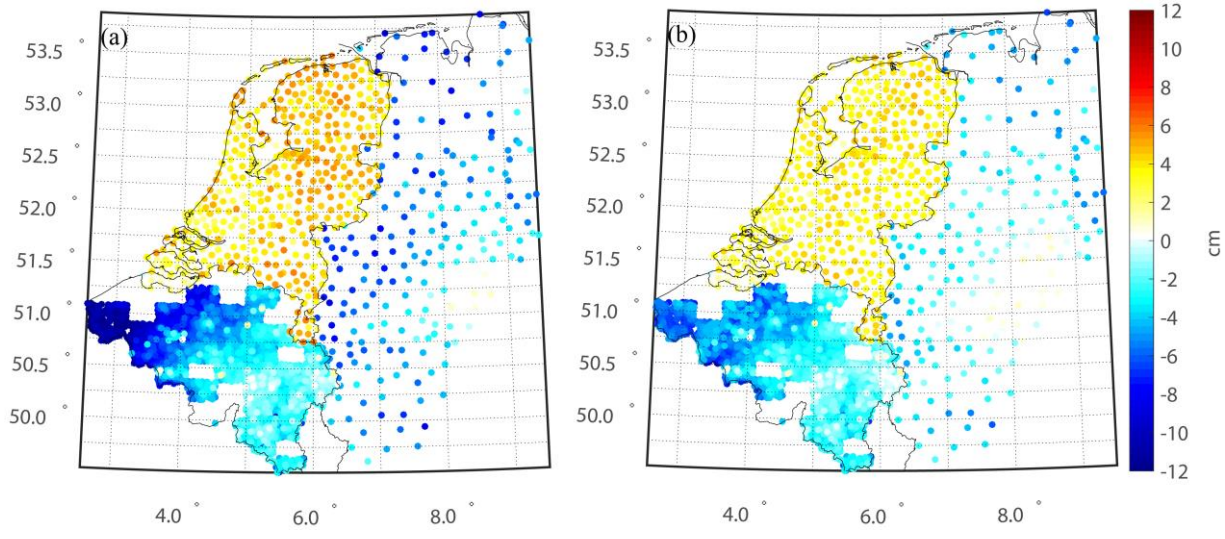


Figure 7. Differences between GPS/leveling data and gravimetric quasi-geoids computed from (a) single-layer and (b) multilayer approach

Table 6 Evaluation of quasi-geoids modeled from different approaches (Units: cm)

| | | max | min | mean | sd |
|---|---|---|---|---|---|
| Single-layer approach | Netherlands | 5.9 | 0.1 | 3.8 | 1.2 |
| | Belgium | 1.2 | -13.1 | -3.5 | 2.8 |
| | Germany | 6.2 | -11.2 | -3.6 | 2.9 |
| Multilayer approach | Netherlands | 4.8 | 0.1 | 3.3 | 0.9 |
| | Belgium | 1.5 | -7.9 | -2.8 | 2.2 |
| | Germany | 0.9 | -10.5 | -2.9 | 2.1 |

QGNSea V1.0 is compared with a regional model called EGG08 (Denker 2013) and other two recently published GGMs, i.e., EGM2008 (d/o 2190) (Pavlis et al. 2012) and EIGEN-6C4 (d/o 2190) (Förste et al. 2014), for cross validation. Differences between QGNSea V1.0and other models are shown in Figure 8, the magnitude of which reaches decimeter level. For EGG08, we note the most prominent differences appear in east parts of the Irish Sea and center of Germany. For EGM2008/EIGEN-6C4, remarkable differences show in south of Norway and northwest of Germany. Apart from the application of different techniques for modeling, these differences are partly interpreted as

Geosci. Model Dev. Discuss., https://doi.org/10.5194/gmd-2017-289
Manuscript under review for journal Geosci. Model Dev.
Discussion started: 17 January 2018




the additional signals introduced by QGNSea V1.0, stemming from the incorporation of more high-quality gravimetry data. The evaluation results displayed in Figure 9 show the quasi-geoid inversed from the multilayer approach has the best quality, especially in the north of the Netherlands and west parts of Belgium, and the accuracies for QGNSea V1.0, EGG08, EGM2008 and EIGEN-6C4 are 1.6 cm, 2.2 cm, 2.6 cm and 2.7 cm, respectively, when comparing with all the GPS/leveling data in the target area (see Table 7). The added values introduced by high-quality data lead to the primary improvements of QGNSea V1.0, which mainly contribute to the fine structures at short-wavelength bands. Moreover, the improvements in the frequency bands that GOCE data contribute may be also the reasons, since EGM2008/EGG08 was developed without GOCE data.

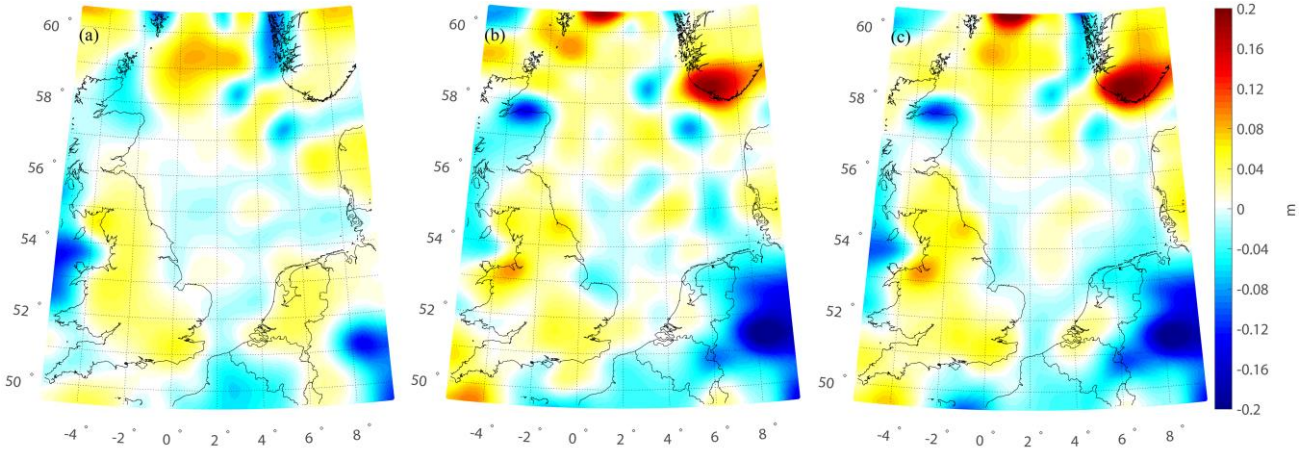


Figure 8. Difference between QGNSea V1.0 and (a) EGG08, (b) EIGEN-6C4, (c) EGM2008. Note that the mean differences are removed.

Geosci. Model Dev. Discuss., https://doi.org/10.5194/gmd-2017-289
Manuscript under review for journal Geosci. Model Dev.
Discussion started: 17 January 2018


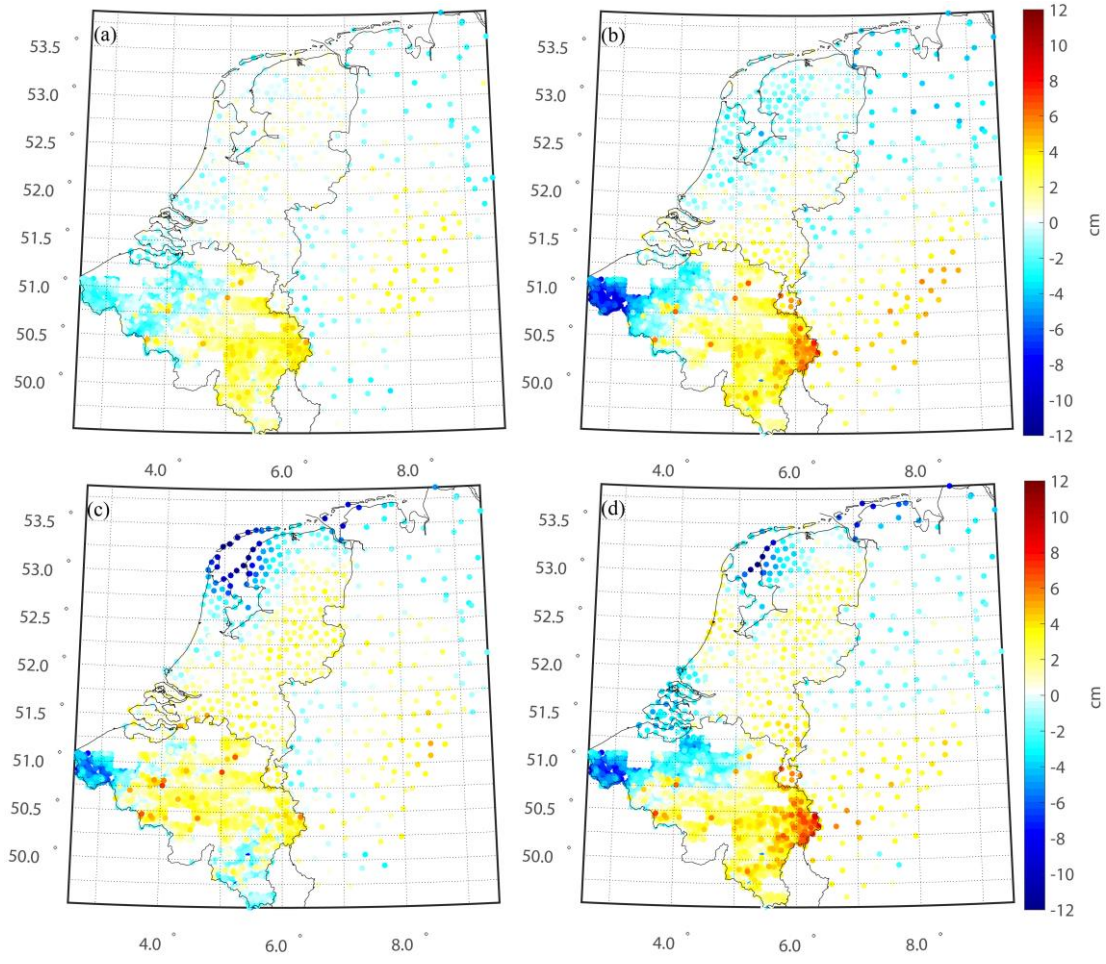


Figure 9. Evaluation of the various quasi-geoids. (a) QGNSea V1.0, (b) EGG08, (c) EGM2008, (d) EIGEN-6C4. Note that the mean differences are removed

Table 7. Statistics of accuracy of various quasi-geoids. (units: cm). Note that the mean differences are removed

| | max | min | sd |
|---|---|---|---|
| QGNSea V1.0 | 5.6 | -4.4 | 1.6 |
| EGG08 | 7.8 | 9.4 | 2.2 |
| EGM2008 | 8.4 | 10.0 | 2.6 |
| EIGEN-6C4 | 9.0 | 11.9 | 2.7 |

For further comparisons, a high-resolution mean dynamic topography (MDT) over the target region is derived using QGNSea V1.0, which is compared with an existing model called DTU13MDT with the spatial resolution of 1′×1′

Geosci. Model Dev. Discuss., https://doi.org/10.5194/gmd-2017-289
Manuscript under review for journal Geosci. Model Dev.
Discussion started: 17 January 2018




(Figure 10 (b)). Similar as the methods for computing DTU13MDT (Andersen et al., 2013), the local MDT is computed in a purely geodetic way, where DTU13MSS and QGNSea V1.0 are directly combined, and a Gaussian filter with a correlation length of 75 km is further applied to smooth the derived MDT. The modeled MDT called NSeaMDT (Mean dynamic topography over the North Sea) is displayed in Figure 10 (a), showing in good agreement with DTU13MDT in most areas over the North Sea. Although the misfit between QGNSea V1.0 and EGM2008 reaches several centimeters in the North Sea (see Figure 8 (c)), the applied Gaussian filter seems attenuates these differences and consequently, these two MDTs demonstrate similar structures in the spatial domain. It is also worth noting that observable differences appear between these MDTs, especially in the northern parts of the North Sea and east parts of the Irish Sea. The geostrophic velocities in Figure 11 indicate the geostrophic surface currents are rather smooth in the North Sea, where the SD values for the zonal (meridian) components are approximately 1.96 cm/s (1.86 cm/s) and the absolute values for both the zonal and meridian components are within 8 cm/s in the open sea areas. Similar results can also be found in Hipkin et al. (2004).

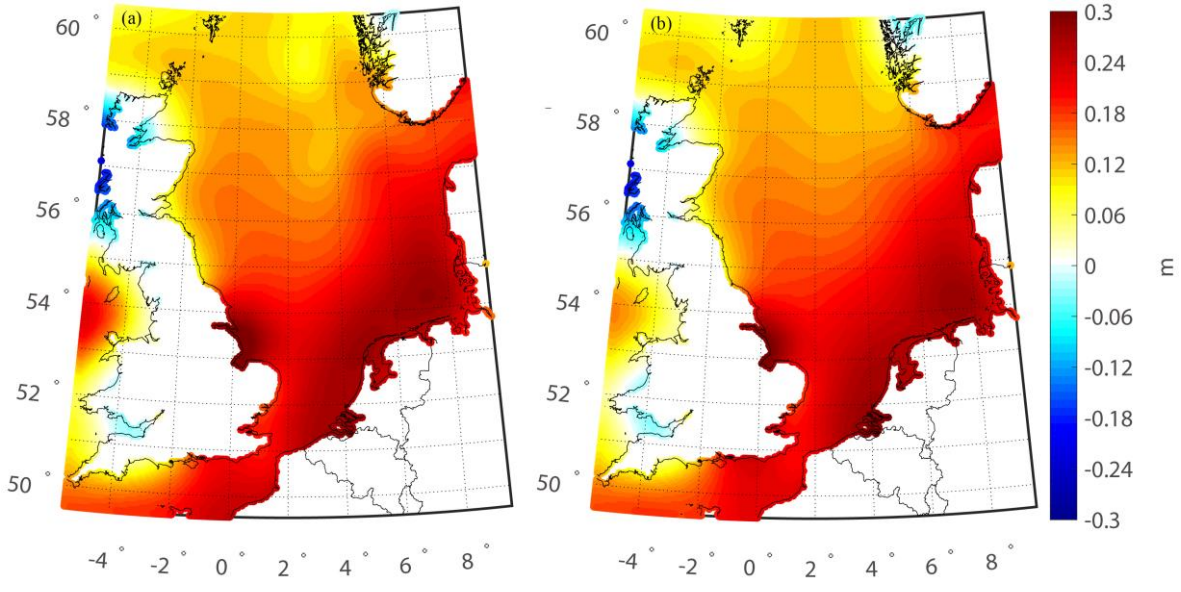


Figure 10. Different mean dynamic topography models. (a) NSeaMDT; (b) DTU13MDT

Geosci. Model Dev. Discuss., https://doi.org/10.5194/gmd-2017-289
Manuscript under review for journal Geosci. Model Dev.
Discussion started: 17 January 2018


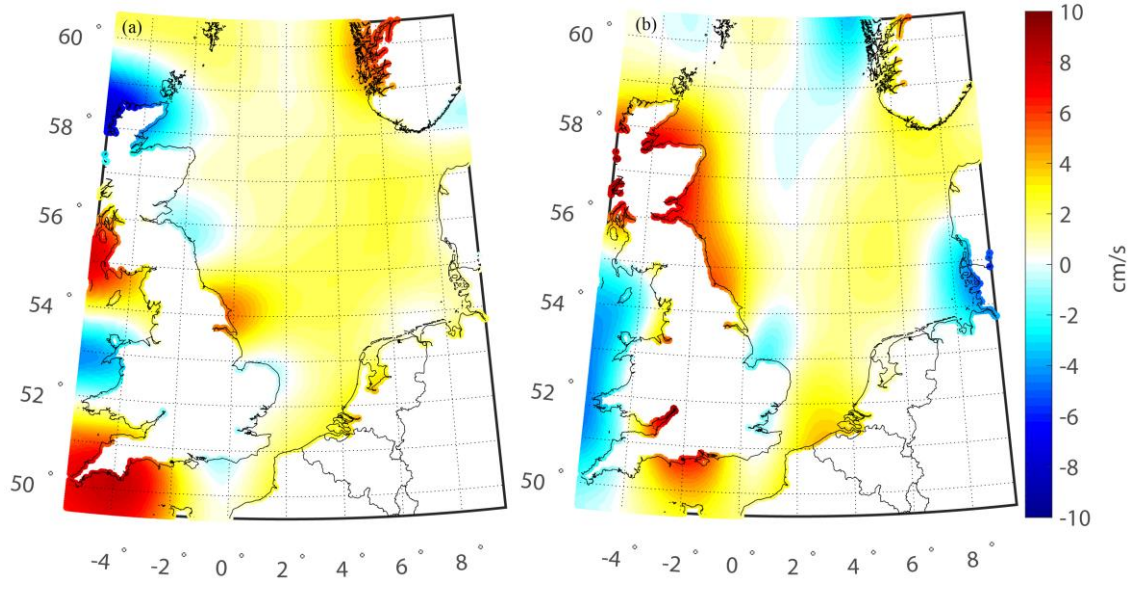


Figure 11. Geostrophic (a) zonal and (b) meridian velocities associated with the NSeaMDT

## 4. Conclusions

A multilayer approach is developed for gravity field recovery at regional scales from heterogeneous data based on the idea of multi-resolution representation, where the residual gravity field is parameterized as the superposition of the Poisson wavelets' grids located at the different depths beneath the topography. Since the gravity signals is the sum of the contributions generated from the anomaly sources at different depths, we put the multiply layers at the locations where different anomaly sources situate. Further, wavelet decomposition and power spectrum analysis are applied for estimating the depths of different layers.

For testing the performance of this multilayer approach, a local gravimetric quasi-geoid called QGNSea V1.0 over the North Sea in Europe is modeled and compared with other models, where a dense coverage of high-quality measurements extending continuously from land to ocean are available. Based on wavelet analysis, multiply layers that situate between 5.7 km and 60.1 km underneath the topography are built to capture the signals with different spectral contents. The numerical results show that the multilayer approach is sensitive to the spectrum of signals, both in the low- and high-frequency bands. The comparison with the single-layer approach show that the residuals of data derived from the multilayers approach reduce significantly in the target area, especially in the regions where the gravity signals show strong correlations with the variation of local topography. The evaluation with GPS/leveling data reveals the



multilayer approach deriving a more accurate quasi-geoid, where QGNSea V1.0 outperforms the solution obtained by the single-layer approach, by the magnitudes of 0.3, 0.6 and 0.8 cm in the Netherlands, Belgium and parts of Germany, respectively. Further comparison with the existing models indicates that QGNSea V1.0 has the best performance, which could be used for investigating the ocean circulation in the local areas.

Future work is needed for further improving the QGNSea V1.0. First, the satellite data (e.g., K-band Range Rate data and gravity gradients) from GRACE and GOCE missions can be combined with the ground-based gravity data for further improving the solution quality. However, deeper Poisson wavelet's grids than ones we use to combine surface data may be implemented to incorporate satellite observations, since these data are more sensitive to low-frequency gravity signals. In addition, the stochastic model may need to be refined. For instance, the effects on the solutions caused by the GGM' errors may be quantified if we incorporate the full error variance-covariance matrix of the spherical coefficients into the stochastic model. Consequently, the different data may be more properly weighted, and the solution can be further improved.

***Author contributions.*** All authors have contributed to designing the approach and writing the manuscript.

***Code and data availability.*** The source code is included as the Supplement. Gravity data were provided by the British Geological Service; the Geological Survey of Northern Ireland; the Nordic Geodetic Commission; Bundesamt für Kartographie und Geodäsie (Germany); Institut für Erdmessung (Germany); the Bureau Gravimétrique International IAG service (France); the Banque de données Gravimétriques de la France; and the Bureau de Recherches Géologiques et Minières (France). GPS/leveling data were provided by the Geo-information and ICT of Rijkswaterstaat (RWS-AGI) and the GPS Kernnet of the Kadaster, National Geographic Institute (NGI) and the Royal Observatory (ROB), and Bundesamt für Kartographie und Geodäsie.

***Competing interests.*** The authors declare that they have no conflict of interest.

***Acknowledgments***. We acknowledge funding from the Netherlands Vertical Reference Frame project. Part of the work was done in Delft University of Technology under the support with the State Scholarship Fund from Chinese Scholarship Council (201306270014). This study was also supported by China Postdoctoral Science Foundation (No.2016M602301) and the Open Research Fund Program of the State Key Laboratory of Geodesy and Earth's Dynamics (Institute of Geodesy and Geophysics, CAS) (Grant No.SKLGED2018-1-2-E).

Geosci. Model Dev. Discuss., https://doi.org/10.5194/gmd-2017-289
Manuscript under review for journal Geosci. Model Dev.
Discussion started: 17 January 2018




## References

Andersen, O. B., Knudsen, P., and Stenseng, L.: The DTU13 global mean sea surface from 20 years of satellite altimetry, In: OSTST Meeting, Boulder, Colo, 2013.

Artemieva, I.M. and Thybo, H.: EUNAseis: A seismic model for Moho and crustal structure in Europe, Greenland, and the North Atlantic region, Tectonophysics, 609, 97-153, doi:10.1016/j.tecto.2013.08.004, 2013.

Audet, P.: Toward mapping the effective elastic thickness of planetary lithospheres from a spherical wavelet analysis of gravity and topography, Phys. Earth. Planet. In., 226(1), 48-82, doi: 10.1016/j.pepi.2013.09.011, 2014.

Bentel, K., Schmidt, M. and Rolstad, D.C.: Artifacts in regional gravity representations with spherical radial basis functions, Journal of Geodetic Science, 3(3), 173-187, doi:10.2478/jogs-2013-0029, 2013

Chambodut, A., Panet, I., Mandea, M., Diament, M., Holschneider, M. and Jamet, O.: Wavelet frames: an alternative to spherical harmonic representation of potential fields, Geophys. J. Int., 163(3), 875-899, doi:10.1111/j.1365-246X.2005.02754.x, 2005.

Cianciara, B. and Marcak, H.: Interpretation of gravity anomalies by means of local power spectra, Geophys. Prospect., 24 (2), 273-286, doi: 10.1111/j.1365-2478.1976.tb00925.x, 1976.

Denker, H.: Regional Gravity Field Modeling: Theory and Practical Results, In: G Xu (ed)Sciences of 641 Geodesy - II, 185-291, Springer, Berlin, Heidelberg, 2013.

Eicker, A., Schall, J. and Kusche, J.: Regional gravity modeling from spaceborne data: case studies with GOCE, Geophys. J. Int., 196(3), 1431-1440, doi:10.1093/gji/ggt485, 2013.

Fengler, M.J., Freeden, W., Kohlhaas, A., Michel, V. and Peters, T.: Wavelet Modeling of Regional and Temporal Variations of the Earth's Gravitational Potential Observed by GRACE, J. Geod., 81(1), 5-15, doi: 10.1007/s00190-006-0040-1, 2007.

Fengler, M.J., Freeden, W. and Michel, V.: The Kaiserslautern multiscale geopotential model SWITCH-03 from orbit perturbations of the satellite CHAMP and its comparison to the models EGM96, UCPH2002_02_0.5, EIGEN-1s and EIGEN-2, Geophys. J. Int., 157(2), 499-514, doi:10.1111/j.1365-246X.2004.02209.x, 2004.

Forsberg, R. and Tscherning, C.C.: An overview manual for the GRAVSOFT geodetic gravity field modeling programs, 2nd edn. National Space Institute, Denmark and Niels Bohr Institute, University of Copenhagen, 2008.

Förste, C., Bruinsma, S.L., Abrikosov, O., Lemoine, J.M., Schaller, T., Götze, H.J., Ebbing, J., Marty, J.C., Flechtner, F., Balmino, G. and Biancale, R.: EIGEN-6C4 The latest combined global gravity field model including GOCE data up

to degree and order 2190 of GFZ Potsdam and GRGS Toulouse. The 5th GOCE User Workshop, Paris, France, 2014.

Freeden, W., Gervens, T. and Schreiner, M.: Constructive Approximation on the Sphere (With Applications to Geomathematics). Oxford Sci. Publ., Clarendon Press, Oxford, 1998.

Freeden, W., Fehlinger, T., Klug, M., Mathar, D. and Wolf, K.: Classical globally reflected gravity field determination in modern locally oriented multiscale framework. J. Geod., 83, 1171-1191, doi:10.1007/s00190-009-0335-0, 2009.

Freeden, W. and Schreiner, M.: Local multiscale modelling of geoid undulations from deflections of the vertical, J. Geod., 79, 641-651, doi: 10.1007/s00190-005-0017-5, 2006.

Grad, M. and Tiira, T.: TheMoho depthmap of the European Plate. Geophys. J. Int., 176, 279-292, doi:10.1111/j.1365-246X.2008.03919.x, 2009.

Hipkin, R.G., Haines, K., Beggan, C., Bingley, R., Hernandez, F., Holt, J. and Baker, T.: The geoid EDIN2000 and mean sea surface topography around the British Isles, Geophys. J. Int., 157(2), 565-577, doi:10.1111/j.1365-246X.2004.01989.x, 2004.

Holschneider, M. and Iglewska-Nowak, I.: Poisson wavelets on the sphere. J. Fourier. Anal. Appl., 13(4), 405-419, doi:10.1007/s00041-006-6909-9, 2007.

Jiang, W., Zhang, J., Tian, T. and Wang, X.: Crustal structure of Chuan-Dian region derived from gravity data and its tectonic implications, Phys. Earth. Planet. Interiors., 212-213, 76-87, doi: 10.1016/j.pepi.2012.07.001, 2012.

Klees, R., Tenzer, R., Prutkin, I. and Wittwer, T.: A data-driven approach to local gravity field modelling using spherical radial basis functions, J. Geod., 82(8), 457-471, doi:10.1007/s00190-007-0196-3, 2008.

Koch, K.R. and Kusche, J.: Regularization of geopotential determination from satellite data by variance components, J. Geod., 76, 259-268, doi: 10.1007/s00190-002-0245-x, 2002.

Kusche, J.: A Monte-Carlo technique for weight estimation in satellite geodesy, J. Geod., 76(11), 641-652, doi:10.1007/s00190-002-0302-5, 2003.

Lieb, V., Schmidt, M., Dettmering, D. and Börger, K.: Combination of various observation techniques for regional modeling of the gravity field, J. Geophys. Res. Solid Earth, 121, 3825-3845, doi:10.1002/2015JB012586, 2016.

Mayer-Gürr, T., Pail, R., Gruber, T., Fecher, T., Rexer, M., Schuh, W.-D., Kusche, J., Brockmann, J.-M., Rieser, D., Zehentner, N., Kvas, A., Klinger, B., Baur, O., Höck, E., Krauss, S., and Jäggi, A.: The combined satellite gravity field model GOCO05s, Geophys Res Abs 17:EGU2015-12364, 2015.

Naeimi, M., Flury, J. and Brieden, P.: On the regularization of regional gravity field solutions in spherical radial base functions, Geophys. J. Int., 202, 1041-1053, doi:10.1093/gji/ggv210, 2015.

Omang, O.C.D. and Forsberg, R.: How to handle topography in practical geoid determination: three examples, J. Geod., 74(6), 458-466, doi:10.1007/s001900000107, 2000.

Panet, I., Kuroishi, Y. and Holschneider, M.: Wavelet modelling of the gravity field by domain decomposition methods: an example over Japan, Geophys. J. Int., 184(1), 203-219, doi:10.1111/j.1365-246X.2010.04840.x, 2011.

Pavlis, N.K., Holmes, S.A., Kenyon, S.C. and Factor, J.F.: The development and evaluation of Earth Gravitational Model (EGM2008), J. Geophys. Res., 117, B04406, doi:10.1029/2011JB008916, 2012.

Schmidt, M., Fengler, M., Mayer-Gürr, T., Eicker, A., Kusche, J., Sánchez, L. and Han, S.C.: Regional gravity modeling in terms of sphericalbase functions, J. Geod., 81(1), 17-38, doi:10.1007/s00190-006-0101-5, 2007.

Schmidt, M., Fabert, O., Shum, C.K.: On the estimation of a multi-resolution representation of the gravity field based on spherical harmonics and wavelets, J. Geodyn., 39(1), 512-526, doi: 10.1016/j.jog.2005.04.007, 2005.

Schmidt, M., Han, S.C., Kusche, J., Sanchez, L. and Shum, C.K.: Regional high- resolution spatiotemporal gravity modeling from GRACE data using spherical wavelets, Geophys. Res. Lett., 33, L08403, doi:10.1029/2005GL025509, 2006.

Slobbe, D.C., Klees, R. and Gunter, B.C.: Realization of a consistent set of vertical reference surfaces in coastal areas, J. Geod., 88(6), 601-615, doi:10.1007/s00190-014-0709-9, 2014.

Spector, A. and Grant, F.S.: Statistical models for interpreting aeromagnetic data, Geophysics, 35(2), 293-302, doi:10.1190/1.1440092, 1970.

Syberg, F.J.R.: A Fourier method for the regional-residual problem of potential fields, Geophys. Prospect., 20 (1), 47-75, doi:10.1111/j.1365-2478.1972.tb00619.x, 1972.

Tenzer, R. and Klees, R.: The choice of the spherical radial basis functions in local gravity field modeling. Stud. Geophys. Geod., 52(3), 287-304, doi:10.1007/s11200-008-0022-2, 2008.

Tenzer, R., Klees, R. and Wittwer, T.: Local Gravity Field Modelling in Rugged Terrain Using Spherical Radial Basis Functions: Case Study for the Canadian Rocky Mountains. In S. Kenyon, Geodesy for Planet Earth, International Association of Geodesy Symposia 136, Springer-Verlag Berlin Heidelberg, pp 401-409, 2012.

Wittwer, T.: Regional gravity field modelling with radial basis functions, Dissertation, Delft University of Technology, Delft, The Netherlands, 2009.

Wu, Y., Luo, Z., Chen, W. and Chen, Y.: High-resolution regional gravity field recovery from Poisson wavelets using heterogeneous observational techniques, Earth Planets Space, 69:34, doi:10.1186/s40623-017-0618-2, 2017a.

Wu, Y., Luo, Z. and Zhou, B.: Regional gravity modelling based on heterogeneous data sets by using Poisson wavelets

radial basis functions, Chin. J. Geophys (in Chinese), 59(3):852-864, doi:10.6038/cjg20160308, 2016.

Wu, Y., Zhou, H., Zhong, B., and Luo, Z.: Regional gravity field recovery using the GOCE gravity gradient tensor and heterogeneous gravimetry and altimetry data, J. Geophys. Res. Solid Earth, 122(8), 6928-6952, doi: doi:10.1002/2017JB014196, 2017b.

Xu, C., Liu, Z., Luo, Z., Wu, Y. and Wang, H.: Moho topography of the Tibetan Plateau using multi-scale gravity analysis and its tectonic implications, J. Asian. Earth. Sci., 138, 378-386, doi: 10.1016/j.jseaes.2017.02.028, 2017.